


Collisional-radiative modeling of the $5p$ - $5s$ spectrum of W XIV–W XVI ions

Xiaobin Ding ^{1,*}, Fengling Zhang,¹ Yang Yang,² Ling Zhang,³ Fumihiro Koike,⁴ Izumi Murakami,^{5,6} Daiji Kato,^{5,7} Hiroyuki A. Sakaue,⁵ Nobuyuki Nakamura,⁸ and Chenzhong Dong¹

¹Key Laboratory of Atomic and Molecular Physics and Functional Materials of Gansu Province, College of Physics and Electronic Engineering, Northwest Normal University, Lanzhou 730070, China

²Key Laboratory of Applied Ion Beam Ministry of Education, Institute of Modern Physics, Fudan University, Shanghai 200433, China

³Institute of Plasma Physics, Chinese Academy of Sciences, Hefei 230000, China

⁴Department of Physics, Sophia University, Tokyo 102-8554, Japan

⁵National Institute for Fusion Science, National Institutes of Natural Sciences, Toki, Gifu 509-5292, Japan

⁶Department of Fusion Science, The Graduate University for Advanced Studies, SOKENDAI, Toki, Gifu 509-5292, Japan

⁷Department of Advanced Energy Engineering Science, Kyushu University, Fukuoka 816-8580, Japan

⁸Institute for Laser Science, The University of Electro-Communications, Chofu, Tokyo 182-8585, Japan



(Received 5 January 2020; revised manuscript received 11 March 2020; accepted 25 March 2020; published 27 April 2020)

The wavelength and rate of the $5p$ - $5s$ transition of W XIV–W XVI ions have been calculated by the relativistic configuration interaction method with the implementation of the flexible atomic code. A reasonable collisional-radiative model has been constructed to simulate the $5p$ - $5s$ transition spectrum of W XIV–W XVI ions, which had been observed in the electron beam ion trap device. The results are in reasonable agreement with the available experimental and theoretical data, which might be applied to identify the controversial spectra. The confusion on the assignment of the ionization stage is solved in the present work.

DOI: [10.1103/PhysRevA.101.042509](https://doi.org/10.1103/PhysRevA.101.042509)

I. INTRODUCTION

Tungsten is selected as the divertor and plasma-facing material for magnetic confinement fusion devices, such as ITER and EAST, due to its high melting point and high sputtering energy threshold, low sputtering rate, and low deuterium and tritium retention rate [1,2]. However, due to the interaction between the edge plasma and the wall material, tungsten might be ionized and transported to the high-temperature core plasma region and be ionized further. Therefore, tungsten ion may exist as the intrinsic impurities both in the plasma core and edge region. Significant radiation power loss caused by highly charged tungsten ions will lead to the degradation of the plasma performance or even plasma disruption if the relative concentration of tungsten ions in the core plasma is higher than 10^{-5} [3]. Quantitative diagnostics of tungsten influx and concentration are crucial to understanding the tungsten transport in fusion plasma. Furthermore, the control of tungsten impurity is one of the critical issues of the steady-state operation of the future fusion reactor. On the other hand, a tiny amount of tungsten ion is beneficial to diagnose the plasma parameters such as temperature and density of fusion plasma. Therefore, knowledge of the atomic structure, properties, kinetic process, and emission spectra of various tungsten ions is required and is expected to have great significance for the diagnosis of fusion plasma.

The highly ionized tungsten ion has a relatively simple structure and has been widely studied [4–13]. For the tungsten

ions with a lower degree of ionization, many studies on its spectral line can also be found [14–24]. However, the data of tungsten ion with a moderate ionization degree is still relatively lacking, especially for the data of W VIII–WXXVIII ions [25,26]. These tungsten ions have several electrons on the open $4f$ shell, which makes their spectra complex and challenging to explain. Meanwhile, the theoretical calculation on the atomic structure and spectrum is complicated due to the influence of the $4f$ wave function collapse. Also, relativistic effects and electron-correlation effects in these ions have a significant influence on their structure and transition properties, especially on their ground and low-lying excited state [27–29].

Electron beam ion trap (EBIT) is now being widely used to observe the spectrum of the tungsten ions [19,22,30–35]. By observing the dependence of the spectrum intensity on the incident electron beam energy, the spectrum could be assigned to the appropriate ions. Therefore, it provides plenty of knowledge on the transitions and atomic properties of tungsten ions.

In 2015, Li *et al.* measured the extreme ultraviolet (EUV) spectra of W^{11+} - W^{15+} on Shanghai EBIT [36]. They assigned the lines in 24.62–25.22 nm, 24.32–24.92 nm, 23.27–24.09 nm, 22.54–23.37 nm, and 21.48–22.69 nm to the $5p$ - $5s$ transition of W^{11+} - W^{15+} ions, respectively. In the same year, Kobayashi *et al.* measured the EUV and visible spectra of W^{12+} - W^{14+} ions on Tokyo EBIT [37]. They thought that the lines at 24.32, 24.77, 24.83, and 24.91 nm are the $5p$ - $5s$ transition of the W^{13+} ion, while the lines in 23.27–24.09 nm are from the W^{14+} ion. The identification of the ionization degree, from these two independent works, is different by one

*dingxb@nwnu.edu.cn

ionization state. The $5p$ - $5s$ spectra of the W^{13+} – W^{15+} ions were calculated by the collisional-radiative model to clarify the confusion on the spectrum identification in the paper.

II. THEORETICAL METHOD

A collisional-radiative model (CRM) has been widely used to simulate and explain the observed plasma spectrum [19,22,30–32,36,38–45]. The spectral intensity $I_{p,q}(\lambda)$ of a transition with wavelength λ from the upper excited level p to the lower level q can be expressed by

$$I_{p,q}(\lambda) \propto n(p)A(p, q)\phi(\lambda), \quad (1)$$

where $A(p, q)$ is the radiative transition rate or Einstein coefficient of the transition from p to q , which can be obtained accurately by experimental observation or theoretical calculation. The function $\phi(\lambda)$ is the normalized line profile, which was taken as a Gaussian profile to include the Doppler, natural, collisional, and instrumental broadening effects in the present work. $n(p)$ is the population of the upper excited level p , which was determined by the atomic processes in the plasma and can be obtained by solving the rate equation. To construct the rate equation, the most important atomic processes in the plasma, such as spontaneous radiative transitions, collision excitation and deexcitation, impact ionization, radiation recombination, and three-body recombination, etc., should be taken into account.

In the EBIT, the electron beam energy is assumed to be a monoenergetic distribution. The ionization degree of the ions generated in the ion trap is relatively simple [46]. The low-density plasma in the EBIT can be regarded as optically thin and isotropic, and its ionization and recombination process is much slower than the collisional and radiative processes. Thus, the impact ionization, radiation recombination, three-body recombination, and charge exchange processes are ignored in the present work. The following rate equation can be used to describe the population of the excited upper levels p :

$$\begin{aligned} \frac{d}{dt}n(p) = & \sum_{q>p} F(q, p)n_e n(q) + \sum_{p<q} [C(q, p)n_e + A(q, p)]n(q) \\ & - \left[\sum_{q>p} C(p, q)n_e + \sum_{q<p} F(p, q)n_e + \sum_{p>q} A(p, q) \right] \\ & \times n(p), \end{aligned} \quad (2)$$

where n_e is the electron density of the plasma, $C(p, q)$ and $F(q, p)$ are the collisional excitation and deexcitation rate coefficients from the level p to q , respectively. These rate coefficients can be obtained by convoluting the cross section of the collision excitation (deexcitation) with the free electron energy distribution function, which can be described by the δ function for the monoenergetic electron beam of EBIT. The collision excitation cross section can be obtained by the distorted wave approximation, and the collision deexcitation cross section can be obtained according to the principle of the detailed balance. The first and second terms in the righthand side of Eq. (2) refer to the population flux from the other energy levels to the level p , and the third term represents the depopulation flux from the level p to the other levels.

TABLE I. Configurations included in the CRM and correlation configurations of W^{13+} – W^{15+} .

W^{13+}	W^{14+}	W^{15+}
Configurations included in the CRM		
$4f^{13}5s^2$	$4f^{12}5s^2$	$4f^{11}5s^2$
$4f^{13}5s5p$	$4f^{12}5s5p$	$4f^{11}5s5p$
$4f^{13}5s5d$	$4f^{11}5s^25p$	$4f^{10}5s^25p$
$4f^{12}5s^25p$	$4f^{11}5s5p^2$	$4f^{11}5s^25d$
$4f^{12}5s^25d$		
$4f^{12}5s5p^2$		
Correlation configurations		
$4f^{14}5s$	$4f^{12}5s5d$	$4f^{12}5s$
$4f^{14}5p$	$4f^{11}5s^25d$	$4f^{11}5p^2$
$4f^{14}5d$	$4f^{13}5s$	$4f^{11}5p5d$
$4f^{13}5s5f$	$4f^{13}5p$	$4f^{11}5s5d$
$4f^{13}5s5g$	$4f^{13}5d$	$4f^{11}5s6p$
$4f^{13}5s5d$	$4f^{12}5p5d$	$4f^{11}5s6f$
$4f^{13}5p^2$	$4f^{12}5f^2$	$4f^{10}5s^26d$
$4f^{13}5p5d$	$4f^{10}5s^25f^2$	$4f^{12}5p$
$4f^{13}5p5f$	$4f^{14}$	$4f^{12}5d$
$4f^{13}5p5g$		
$4f^{13}5d^2$		
$4f^{13}5d5f$		
$4f^{13}5d5g$		
$4f^{13}5f^2$		
$4f^{12}5f5g$		
$4f^{13}5g^2$		

The rate equation can be solved in the quasi-steady-state approximation $\frac{d}{dt}n(p) = 0$.

For heavy ions such as tungsten ($Z = 74$), relativistic effects and electron-correlation effects have an essential influence on its structure and transition properties. Therefore, the relativistic configuration interaction method (RCI) was used with the implementation of the flexible atomic code (FAC) [47]. The Dirac-Coulomb Hamiltonian was used, and the low-frequency Breit interaction effect, vacuum polarization, and self-energy corrections were also included in the present calculation. The atomic data, including the energy levels, radiative transition rates, and cross sections of collisional excitation, are calculated. The configurations included in the CRM and the correlation configurations of W^{13+} – W^{15+} ions are given in Table I. By checking the convergence of the total energy of each level with the increase of interaction configuration space, the most significant electron correlation effects were captured in the present calculation. Furthermore, most of the lower level have 90% purity of the eigenfunction. Some of the highly excited states are vigorously mixed with the largest purity of eigenfunction approximate to 40%. However, for simplicity, the leading terms with the largest configuration state components of each level were used to designate the level.

The consistency of the transition rate calculated from dipole length and velocity gauge could also indicate the validity of the calculation results to some extent. For the strong $E1$ transitions, the ratio of the rate calculated in two gauges mostly lies between 1.03 and 1.32. This indicates that our

TABLE II. Excitation energy (in eV) of the first excited state $[(4f_{5/2}^5)_{5/2}5s^2]_{5/2}$ in W^{13+} .

Level	Present	MR-MP [29]	Ref. [39]	Ref. [37]
$(4f_{5/2}^5)_{5/2}$	2.2467	3.1896	2.2545 ^a 2.2461 ^b	2.2124 ^a 2.1836 ^c

^aExperimental results.^bRCI calculation with FAC.^cMCDF + RCI calculation with GRASP2K.

calculations are sufficiently reliable. For brevity, the transition rates were only given in the dipole length gauge in this paper.

III. RESULTS AND DISCUSSION

A. The transition and spectrum of W^{13+} ion

The ground configuration of the W^{13+} ion is $4f^{13}5s^2$, which splits into $[(4f_{5/2}^5)_{5/2}5s^2]_{5/2}$ and $[(4f_{7/2}^7)_{7/2}5s^2]_{7/2}$ doublet levels, while $[(4f_{7/2}^7)_{7/2}5s^2]_{7/2}$ is the ground level. The notations given in here are in relativistic form with the full relativistic orbital omitted. The excitation energy of the first excited state is presented in Table II compared with the existing data from the calculation and experiment. The results calculated using the multireference model potential (MR-MP) theory by Vilkas *et al.* is quite different from both the experimental observation and the theoretical calculation, mainly because the former is the theory using empirical model potentials. Such deviations might be due to inappropriate choices of the experimental values for the model potential, as we found in the previous work [48]. The present RCI calculation is in good agreement with the results, both experimental and calculated by Zhao *et al.* [39]. There is still little difference between the result by Kobayashi *et al.*, and others [37]. Further investigations are expected to solve this difference.

The calculated transition wavelength and transition rates of $5d$ - $5p$ and $5p$ - $5s$ transitions of the W^{13+} ion are presented in Table III with the values of other theories and experiments. For the transition $5d$ - $5p$, only the transitions with a high transition rate are provided.

TABLE III. Wavelength λ (in nanometers) and the transition rate $A_{(p,q)}$ (in $10^{11} s^{-1}$) of $5d$ - $5p$ and $5p$ - $5s$ of the W^{13+} ion. The column ‘‘Key’’ corresponds to the label in Fig. 1.

Key	Lower	Upper	λ	$\lambda_{\text{expt. [37]}}$	$A_{(p,q)}$
	$[(4f_{5/2}^5 4f_{7/2}^7)_{6,5} p_{1/2}]_{13/2}$	$[(4f_{5/2}^5 4f_{7/2}^7)_{6,5} d_{3/2}]_{15/2}$	18.18		1.26
	$[(4f_{7/2}^6)_{6,5} p_{3/2}]_{15/2}$	$[(4f_{7/2}^6)_{6,5} d_{5/2}]_{17/2}$	21.03		1.52
	$[(4f_{5/2}^5 4f_{7/2}^7)_{5,5} p_{3/2}]_{13/2}$	$[(4f_{5/2}^5 4f_{7/2}^7)_{5,5} d_{5/2}]_{15/2}$	21.05		1.49
	$[(4f_{5/2}^4)_{4,5} p_{3/2}]_{11/2}$	$[(4f_{7/2}^4)_{4,5} d_{5/2}]_{13/2}$	21.07		1.41
	$[(4f_{5/2}^5 4f_{7/2}^7)_{5,5} p_{3/2}]_{15/2}$	$[(4f_{5/2}^5 4f_{7/2}^7)_{6,5} d_{5/2}]_{17/2}$	21.13		1.50
1	$[(4f_{5/2}^5)_{5/2} 5s^2]_{5/2}$	$\{[(4f_{5/2}^5)_{5/2} 5s_{1/2}]_3 5p_{3/2}\}_{5/2}$	24.09	23.87 ^a 24.00 ^b	0.62 0.63 ^a
2	$[(4f_{7/2}^7)_{7/2} 5s^2]_{7/2}$	$\{[(4f_{7/2}^7)_{7/2} 5s_{1/2}]_4 5p_{3/2}\}_{7/2}$	24.17	23.95 ^a 24.06 ^b	0.55 0.54 ^a
3	$[(4f_{5/2}^5)_{5/2} 5s^2]_{5/2}$	$\{[(4f_{5/2}^5)_{5/2} 5s_{1/2}]_2 5p_{3/2}\}_{7/2}$	24.61	24.41 ^a 24.57 ^b	0.53 0.51 ^a
4	$[(4f_{7/2}^7)_{7/2} 5s^2]_{7/2}$	$\{[(4f_{7/2}^7)_{7/2} 5s_{1/2}]_3 5p_{3/2}\}_{9/2}$	24.69	24.53 ^a 24.64 ^b	0.55 0.61 ^a
5	$[(4f_{7/2}^7)_{7/2} 5s^2]_{7/2}$	$\{[(4f_{7/2}^7)_{7/2} 5s_{1/2}]_4 5p_{3/2}\}_{5/2}$	24.76	24.71 ^a 24.70 ^b	0.57 0.54 ^a
6	$[(4f_{5/2}^5)_{5/2} 5s^2]_{5/2}$	$\{[(4f_{5/2}^5)_{5/2} 5s_{1/2}]_3 5p_{3/2}\}_{3/2}$	24.93		0.58

^aFrom Kobayashi *et al.* with the HULLAC code [37].^bFrom Safronova *et al.* with the Hartree-Fock-relativistic method (COWAN code) [49].

The calculated transition with wavelengths of 17.0–22.00 nm dominated by $5d$ - $5p$ from $4f^{12}5s^25d$ to $4f^{12}5s^25p$. These transitions have a high transition rate but have not been observed in the EBIT experiment [37]. The observed spectrum by EBIT in the wavelengths of 24.00–25.00 nm corresponds to the calculated $5p$ - $5s$ transitions from $4f^{13}5s5p$ to $4f^{13}5s^2$. Compared to the calculated wavelength with the four experimental lines measured by Kobayashi *et al.* in the EBIT, the present calculation discrepancies are 0.62%, 0.65%, 0.56%, and 0.60%; the discrepancies for Kobayashi *et al.* [37] are 1.52%, 1.45%, 1.21%, and 0.80%, and for Safronova *et al.* [49] they are 1.07%, 0.81%, 0.77%, and 0.84%, respectively. By comparison, it can be found that the current calculation results make a better agreement with the experimental values.

The calculated and experimental spectra of the W^{13+} ion in the range of 17.0–27.0 nm is shown in Fig. 1. The upper panel, Fig. 1(a), is the calculated radiative transition rate; the middle panel, Fig. 1(b), is the spectral intensity calculated by the CRM with the electron density $n_e = 10^{10} \text{ cm}^{-3}$ and the incident electron beam energy $E_e = 280 \text{ eV}$; and the bottom panels, Figs. 1(c) and 1(d), are the experimental spectra measured by Kobayashi *et al.* and Li *et al.* on the EBIT device with the electron density $n_e = 10^{10} \text{ cm}^{-3}$ and the electron beam energy $E_e = 280$ and 270 eV [36,37], respectively. In the figure, each individual transition was assumed to have the Gaussian profile with the full width at half maximum (FWHM) 0.03 nm, which corresponds to the experimental resolution. The theoretical transition wavelengths are shifted to longer wavelengths by 0.15 nm to compare with the experimental spectra. The peaks in wavelengths of 23.00–23.62 nm are mainly from $4f^{12}5s5p^2$ to $4f^{12}5s^25p$ transition, and the wavelengths of 24.00–25.00 nm are from $4f^{13}5s5p$ to $4f^{13}5s^2$ transition. As can be seen from the figure, the transitions near 20.86–21.17 nm have a large rate [Fig. 1(a)], but it has not been observed in the experiment both in Figs. 1(c) and 1(d). This might be caused by the population mechanism of the excited upper levels.

In order to analyze the spectral intensity, the transition rates, population flux, and intensity for some selected transitions are given in Table IV. For convenience, the population

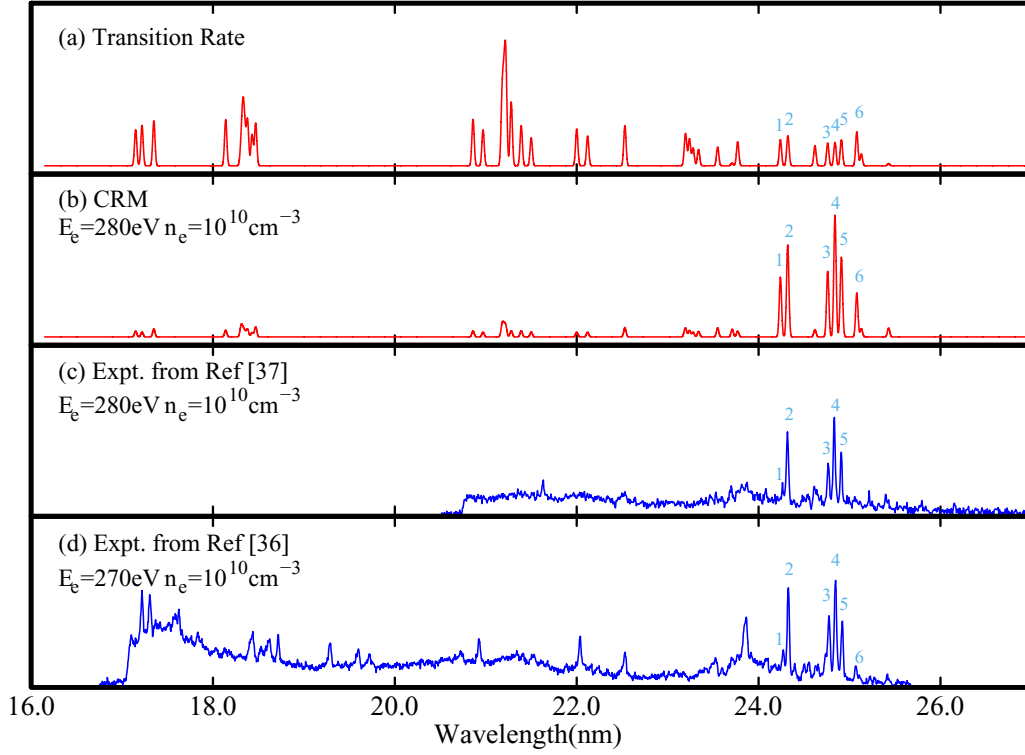


FIG. 1. Comparison between the experimental and calculated spectra of a W^{13+} ion. (a) The calculated radiative transition rate (shifted to the right by 0.15 nm). (b) The spectral intensity calculated by the CRM (shifted to the right by 0.15 nm). (c) Experimental spectra measured by Kobayashi *et al.* [37] on the EBIT device with the electron density $n_e = 10^{10} \text{ cm}^{-3}$ and the energy of the electron beam $E_e = 280 \text{ eV}$. (d) Experimental spectra measured by Li *et al.* [36] on the EBIT with the electron density $n_e = 10^{10} \text{ cm}^{-3}$ and the energy of the electron beam $E_e = 270 \text{ eV}$.

flux from collisional deexcitation of the higher levels was given by $I_{F_{in}} = \sum_{q>p} F(q, p)n_e n(q)$, the population flux from collisional excitation of the lower levels was given by $I_{C_{in}} = \sum_{p<q} C(q, p)n_e n(q)$, and the population flux from spontaneous radiation transition of the higher levels was given by $I_{A_{in}} = \sum_{p<q} A(q, p)n(q)$, respectively.

As can be seen from Table IV, the collisional deexcitation flux $I_{F_{in}}$ is generally smaller than the other two processes by 11 orders of magnitude, so that can be ignored. The population

is mainly from the collisional excitation and the spontaneous radiative transition. For the excited $5d$ upper level, its population mainly comes from the collisional excitation of the lower level. Moreover, the spontaneous radiative transition from the upper level is small, because the population of the higher level is very small or even zero. For the excited $5p$ levels, its population mainly comes from the collisional excitation of the lower level and the spontaneous radiation transition of the upper level and $I_{A_{in}}$ cannot be ignored. The collisional

TABLE IV. The total transition rate A_p (in 10^{11} s^{-1}) from upper levels, population flux [$\sum_{q>p} F(q, p)n_e n(q)$, $\sum_{p<q} C(q, p)n_e n(q)$, and $\sum_{p<q} A(q, p)n(q)$] to the upper level represented by $I_{F_{in}}$, $I_{C_{in}}$, and $I_{A_{in}}$, respectively], and intensity Int. (in $10^{-2} \text{ cm}^{-3} \text{ s}^{-1}$) of $5d-5p$ and $5p-5s$ of the W^{13+} ion. $I_{F_{in}}$ is in $10^{-13} \text{ cm}^{-3} \text{ s}^{-1}$; $I_{C_{in}}$ and $I_{A_{in}}$ are in $10^{-2} \text{ cm}^{-3} \text{ s}^{-1}$.

λ	Upper	A_p	$I_{C_{in}}$	$I_{A_{in}}$	$I_{F_{in}}$	Int.
18.18	$[(4f_{5/2}^5 4f_{7/2}^7)_6 5d_{3/2}]_{15/2}$	1.73	6.53	7.73×10^{-12}	1.47	4.77
21.03	$[(4f_{7/2}^6)_6 5d_{5/2}]_{17/2}$	1.52	9.48	0	3.21	9.48
21.05	$[(4f_{5/2}^5 4f_{7/2}^7)_5 5d_{5/2}]_{15/2}$	1.53	6.87	0	5.74	6.66
21.07	$[(4f_{7/2}^4)_4 5d_{5/2}]_{13/2}$	1.53	4.27	0	2.53	3.93
21.13	$[(4f_{5/2}^5 4f_{7/2}^7)_6 5d_{5/2}]_{17/2}$	1.50	4.90	0	1.03	4.90
24.09	$\{[(4f_{5/2}^5)_{5/2} 5s_{1/2}]_3 5p_{3/2}\}_{5/2}$	0.64	39.8	8.26	39.3	46.7
24.17	$\{[(4f_{7/2}^7)_{7/2} 5s_{1/2}]_4 5p_{3/2}\}_{7/2}$	0.62	73.8	3.64	28.9	69.4
24.61	$\{[(4f_{5/2}^5)_{5/2} 5s_{1/2}]_2 5p_{3/2}\}_{7/2}$	0.60	55.5	2.50	36.2	51.5
24.69	$\{[(4f_{7/2}^7)_{7/2} 5s_{1/2}]_3 5p_{3/2}\}_{9/2}$	0.56	91.6	4.52	61.3	95.4
24.76	$\{[4f_{7/2}^7]_{7/2} 5s_{1/2}]_4 5p_{3/2}\}_{5/2}$	0.59	58.0	2.07	33.2	59.0
24.93	$\{[(4f_{5/2}^5)_{5/2} 5s_{1/2}]_3 5p_{3/2}\}_{3/2}$	0.68	27.4	3.44	24.9	30.6

TABLE V. Wavelength λ (in nanometers), transition rate $A_{(p,q)}$ (in 10^{10} s^{-1}), and intensity Int (in $\text{cm}^{-3} \text{ s}^{-1}$) from $4f^{12}5s5p$ to $4f^{12}5s^2$ transitions in the W^{14+} ion. The column ‘‘Key’’ corresponds to the label in Fig. 2.

Key	Lower	Upper	λ	$A_{(p,q)}$	Int.
1	$[(4f_{5/2}^5 4f_{7/2}^7)_{5/2} 5s^2]_6$	$\{[(4f_{5/2}^5 4f_{7/2}^7)_{6} 5s_{1/2}]_{13/2} 5p_{3/2}\}_6$	22.83	8.29	2.78
2	$[(4f_{5/2}^5 4f_{7/2}^7)_{5/2} 5s^2]_5$	$\{[(4f_{5/2}^5 4f_{7/2}^7)_{5} 5s_{1/2}]_{11/2} 5p_{3/2}\}_5$	23.19	3.32	1.20
3	$[(4f_{5/2}^5 4f_{7/2}^7)_{5/2} 5s^2]_5$	$\{[(4f_{5/2}^5 4f_{7/2}^7)_{4} 5s_{1/2}]_{7/2} 5p_{3/2}\}_5$	23.28	4.01	1.47
4	$[(4f_{7/2}^6)_{6} 5s^2]_6$	$\{[(4f_{7/2}^6)_{6} 5s_{1/2}]_{11/2} 5p_{3/2}\}_6$	23.32	6.12	3.62
	$[(4f_{5/2}^4)_{2} 5s^2]_2$	$\{[(4f_{5/2}^4)_{2} 5s_{1/2}]_{3/2} 5p_{3/2}\}_3$	23.34	6.84	1.07
5	$[(4f_{7/2}^6)_{2} 5s^2]_2$	$\{[(4f_{7/2}^6)_{2} 5s_{1/2}]_{3/2} 5p_{3/2}\}_3$	23.37	5.41	1.10
6	$[(4f_{5/2}^5 4f_{7/2}^7)_{5/2} 5s^2]_4$	$\{[(4f_{7/2}^6)_{6} 5s_{1/2}]_{11/2} 5p_{3/2}\}_7$	23.40	7.35	1.60
	$[(4f_{5/2}^5 4f_{7/2}^7)_{5/2} 5s^2]_3$	$\{[(4f_{5/2}^5 4f_{7/2}^7)_{3} 5s_{1/2}]_{5/2} 5p_{3/2}\}_4$	23.40	6.14	1.66
7	$[(4f_{7/2}^6)_{4} 5s^2]_4$	$\{[(4f_{7/2}^6)_{4} 5s_{1/2}]_{7/2} 5p_{3/2}\}_5$	23.53	5.82	2.69
8	$[(4f_{5/2}^5 4f_{7/2}^7)_{5/2} 5s^2]_4$	$\{[(4f_{5/2}^5 4f_{7/2}^7)_{4} 5s_{1/2}]_{7/2} 5p_{3/2}\}_5$	23.60	4.09	1.48
9	$[(4f_{7/2}^6)_{4} 5s^2]_4$	$\{[(4f_{7/2}^6)_{4} 5s_{1/2}]_{9/2} 5p_{3/2}\}_3$	23.65	6.13	1.80
10	$[(4f_{5/2}^5 4f_{7/2}^7)_{5/2} 5s^2]_4$	$\{[(4f_{5/2}^5 4f_{7/2}^7)_{5} 5s_{1/2}]_{11/2} 5p_{3/2}\}_5$	23.69	6.20	1.34
	$[(4f_{5/2}^5 4f_{7/2}^7)_{5/2} 5s^2]_3$	$\{[(4f_{5/2}^5 4f_{7/2}^7)_{3} 5s_{1/2}]_{7/2} 5p_{3/2}\}_3$	23.69	4.34	1.62
	$[(4f_{7/2}^6)_{6} 5s^2]_6$	$\{[(4f_{5/2}^6)_{6} 5s_{1/2}]_{13/2} 5p_{3/2}\}_5$	23.70	2.78	1.02
11	$[(4f_{7/2}^6)_{6} 5s^2]_6$	$\{[(4f_{7/2}^6)_{4} 5s_{1/2}]_{9/2} 5p_{3/2}\}_4$	23.73	5.73	2.73
	$[(4f_{5/2}^5 4f_{7/2}^7)_{5/2} 5s^2]_5$	$\{[(4f_{5/2}^5 4f_{7/2}^7)_{5} 5s_{1/2}]_{9/2} 5p_{3/2}\}_6$	23.74	6.84	1.95
12	$[(4f_{5/2}^4)_{4} 5s^2]_4$	$\{[(4f_{5/2}^6)_{4} 5s_{1/2}]_{7/2} 5p_{3/2}\}_5$	23.81	7.68	5.72
13	$[(4f_{7/2}^6)_{6} 5s^2]_6$	$\{[(4f_{5/2}^6)_{6} 5s_{1/2}]_{11/2} 5p_{3/2}\}_7$	23.88	5.83	3.18
	$[(4f_{5/2}^5 4f_{7/2}^7)_{5/2} 5s^2]_6$	$\{[(4f_{5/2}^5 4f_{7/2}^7)_{6} 5s_{1/2}]_{13/2} 5p_{3/2}\}_5$	23.90	6.65	2.16
	$[(4f_{5/2}^5 4f_{7/2}^7)_{5/2} 5s^2]_6$	$\{[(4f_{5/2}^5 4f_{7/2}^7)_{6} 5s_{1/2}]_{11/2} 5p_{3/2}\}_7$	23.92	4.69	1.09
14	$[(4f_{5/2}^5 4f_{7/2}^7)_{5/2} 5s^2]_4$	$\{[(4f_{5/2}^5 4f_{7/2}^7)_{4} 5s_{1/2}]_{9/2} 5p_{3/2}\}_3$	23.97	6.79	3.08

excitation flux I_{C_m} of the upper level of $5d$ is smaller than that of $5p$. As a result, the population of the $5d$ upper level is smaller than the population of the $5p$ upper level. This is the reason why those lines with a high transition rate could not be observed in the EBIT experiment.

We also calculated the spectra at the same electron beam energy as in the experiment of Li *et al.* [36] and found that the relative intensity of the spectrum of W^{13+} is insensitive to the electron beam energy. It is found that the presently calculated W^{13+} spectrum agrees well with the Kobayashi *et al.* [37] EBIT observation, as well as the observation by Li *et al.* [36], except the assignment of the work by Li *et al.* is a W^{12+} ion instead of a W^{13+} ion.

B. The transition and spectrum of W^{14+} ion

The calculated ground configuration of the W^{14+} ion is $4f^{12}5s^2$. The transition wavelength, transition rate, and intensities of $5p$ - $5s$ of the W^{14+} ion are shown in Table V. The transition in wavelength of 22.50–24.50 nm is $5p$ - $5s$ from $4f^{12}5s5p$ to $4f^{12}5s^2$ and from $4f^{11}5s5p^2$ to $4f^{11}5s^25p$. The transition rate from $4f^{12}5s5p$ is more significant than that of $4f^{11}5s5p^2$ by two orders of magnitude. The experimental observations of Li and Kobayashi both have nine peaks with high intensity in the wavelength range of 22.50–24.50 nm. There are more than 30 transitions with a high transition rate obtained by the present calculation. In Table V, only the transition data of the most intense are given. These lines are close in wavelength, and they have similar intensities. For example, the peaks with wavelengths 23.40 and 23.69 nm are both blended. The observed peaks with the keys 4, 6, and 11

have two components mixed, and the lines with the keys 10 and 13 have three components mixed [36,37].

The experimental and calculated spectra of the W^{14+} ion in the range of 20.0–27.0 nm are shown in Fig. 2. The upper panel, Fig. 2(a), is the calculated radiative transition rate; the middle panel, Fig. 2(b), is the spectral intensity calculated by the CRM with the electron density $n_e = 10^{10} \text{ cm}^{-3}$ and the electron beam energy $E_e = 320 \text{ eV}$; the bottom panels, Figs. 2(c) and 2(d), are the experimental spectra measured by Kobayashi *et al.* and Li *et al.* on the EBIT device with the electron density $n_e = 10^{10} \text{ cm}^{-3}$ and the energy of electron $E_e = 320$ and 310 eV [36,37], respectively, while the experimental spectral resolution is 0.03 nm [37]. Each individual transition was assumed to have the Gaussian profile with the FWHM of 0.03 nm. The theoretical transition wavelengths are shifted to longer wavelengths by 0.10 nm to compare with the experimental spectra. The calculated spectrum of the W^{14+} ion is in agreement with the spectrum of W^{13+} observed by Li *et al.* [36]. The observed intensities of the spectra from Li *et al.* and Kobayashi *et al.* are different [36,37]. For example, the lines with the key 6 and 11 are strong in the work of Li *et al.* [36] but weak in the work of Kobayashi *et al.* [37]. The line 13 is weak in the work of Li *et al.* [36] but strong in the work of Kobayashi *et al.* [37]. The calculated spectrum makes a good general agreement with both experiments; only a few differences were found in the spectral intensity. For example, the lines with the keys 5, 8, and 9 are strong in both experiments, but they are relatively weak in the present calculation. The lines with the keys 1, 2, 3, 13, and 14 are strong in the present calculation, but they are weak in the experiment [36,37]. The lines with the key 7 and 10 are strong in the calculated spectrum, but not observed in the

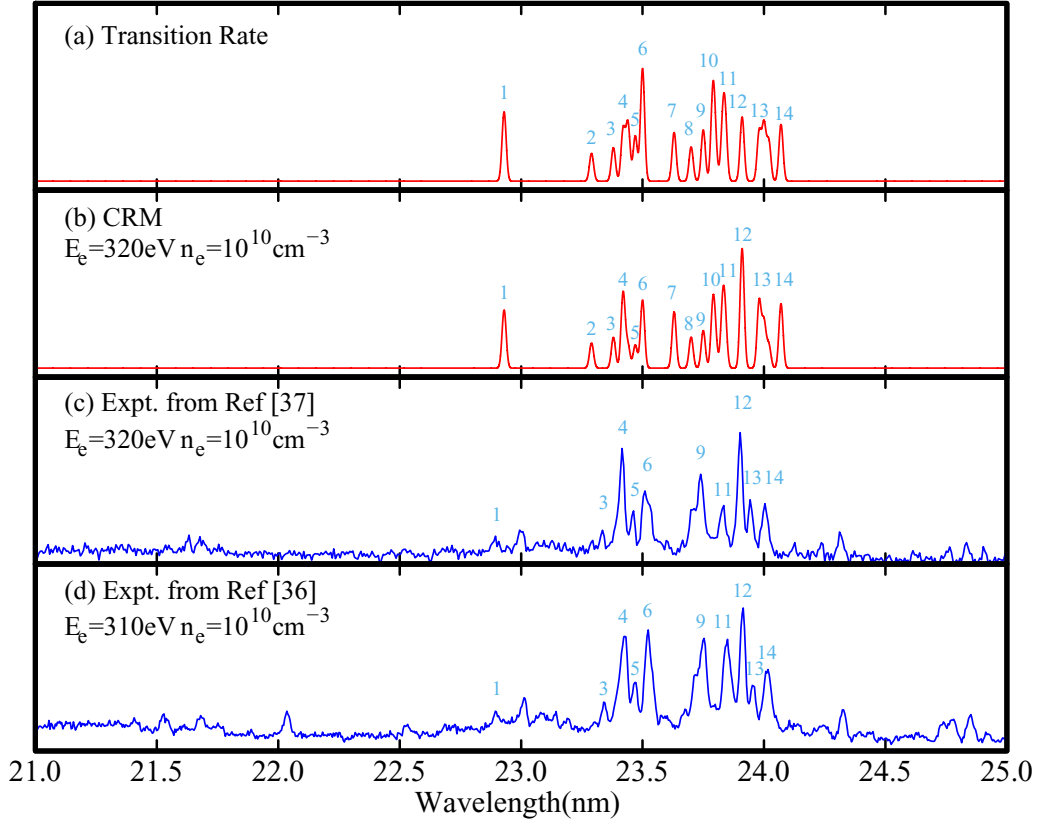


FIG. 2. Comparison between the experimental and calculated spectra of the W^{14+} ion. (a) The calculated radiative transition rate (shifted to the right by 0.10 nm). (b) The spectral intensity calculated by the CRM (shifted to the right by 0.10 nm). (c) Experimental spectra measured by Kobayashi *et al.* on the EBIT device with the electron density $n_e = 10^{10} \text{ cm}^{-3}$ and the energy of electron $E_e = 320 \text{ eV}$. (d) Experimental spectra measured by Li *et al.* [36] on EBIT with $n_e = 10^{10} \text{ cm}^{-3}$ and the energy of electron beam $E_e = 310 \text{ eV}$.

experimental spectrum. These differences need to be studied by further work both experimentally and theoretically.

C. The transition and spectrum of W^{15+} ion

The calculated ground configuration of the W^{15+} ion is $4f^{11}5s^2$. The transition wavelength, transition rate, and spectra intensity of the W^{15+} ion are shown in Table VI. The transition in wavelength at 21.48–22.54 nm is dominated by the $5p$ - $5s$ transition from $4f^{11}5s5p$ to $4f^{11}5s^2$. Similar to the spectrum of W^{14+} , there are six lines with a stronger

intensity in the experimental spectrum of W^{15+} , and there are also more than a dozen of calculated lines with high transition rates. Only the transition data for transitions with high spectra intensity are given in the table. The blended transitions are found in the present calculation. For example, the line with the wavelength 22.70 nm is blended by three components. Moreover, the lines with the keys 2 and 5 have two components mixed.

The synthetic spectrum of the W^{15+} ion is shown in Fig. 3. The upper panel, Fig. 3(a), is the calculated radiative transition

TABLE VI. The transition wavelength λ (in nanometers), transition rate $A_{(p,q)}$ (in 10^{10} s^{-1}), and intensity Int. (in $\text{cm}^{-3} \text{ s}^{-1}$) from $4f^{11}5s5p$ to $4f^{11}5s^2$ transitions in the W^{15+} ion. The column “Key” corresponds to the label in Fig. 3.

Key	Lower	Upper	λ	$A_{(p,q)}$	Int.
1	$[(4f_{7/2}^5)_{15/2}5s^2]_{15/2}$	$\{[(4f_{7/2}^5)_{15/2}5s_{1/2}]_8 5p_{3/2}\}_{15/2}$	22.48	5.89	2.36
2	$[(4f_{7/2}^5)_{11/2}5s^2]_{11/2}$	$\{[(4f_{7/2}^5)_{11/2}5s_{1/2}]_6 5p_{3/2}\}_{11/2}$	22.54	5.59	1.13
	$[(4f_{5/2}^5 4f_{7/2}^6)_{13/2}5s^2]_{13/2}$	$\{[(4f_{5/2}^5 4f_{7/2}^6)_{13/2}5s_{1/2}]_7 5p_{3/2}\}_{13/2}$	22.55	4.26	1.09
3	$[(4f_{7/2}^5)_{15/2}5s^2]_{15/2}$	$\{[(4f_{7/2}^5)_{15/2}5s_{1/2}]_8 5p_{3/2}\}_{13/2}$	22.66	6.20	2.21
4	$[(4f_{7/2}^5)_{9/2}5s^2]_{9/2}$	$\{[(4f_{7/2}^5)_{9/2}5s_{1/2}]_4 5p_{3/2}\}_{11/2}$	22.70	6.74	1.38
	$\{[(4f_{5/2}^4 4f_{7/2}^7)_{11/2}5s^2]_{11/2}\}$	$\{[(4f_{5/2}^4 4f_{7/2}^7)_{11/2}5s_{1/2}]_5 5p_{3/2}\}_{13/2}$	22.70	6.83	1.14
	$[(4f_{7/2}^5)_{11/2}5s^2]_{11/2}$	$\{[(4f_{7/2}^5)_{11/2}5s_{1/2}]_5 5p_{3/2}\}_{13/2}$	22.70	5.13	1.25
5	$[(4f_{5/2}^5 4f_{7/2}^6)_{13/2}5s^2]_{13/2}$	$\{[(4f_{5/2}^5 4f_{7/2}^6)_{13/2}5s_{1/2}]_6 5p_{3/2}\}_{15/2}$	22.77	5.52	1.67
	$[(4f_{7/2}^5)_{15/2}5s^2]_{15/2}$	$\{[(4f_{7/2}^5)_{15/2}5s_{1/2}]_7 5p_{3/2}\}_{17/2}$	22.78	7.63	3.61
6	$[(4f_{5/2}^5 4f_{7/2}^6)_{15/2}5s^2]_{15/2}$	$\{[(4f_{5/2}^5 4f_{7/2}^6)_{15/2}5s_{1/2}]_7 5p_{3/2}\}_{17/2}$	22.92	6.99	1.03

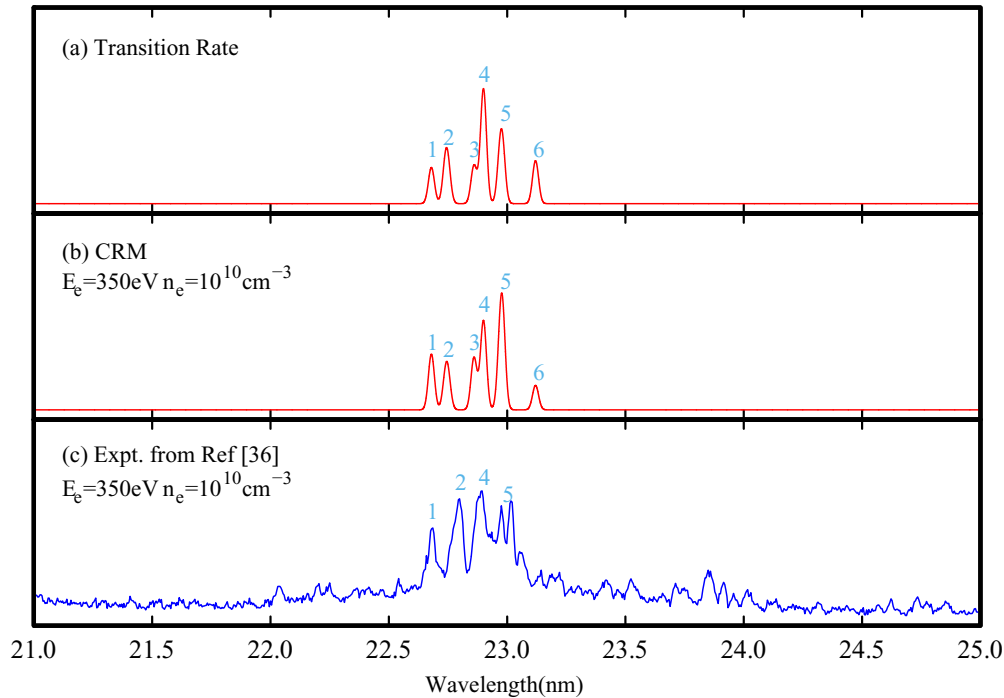


FIG. 3. The synthetic spectrum of the W^{15+} ion. (a) The calculated radiative transition rate. (b) The synthetic spectral intensity calculated by the CRM. (c) Experimental spectra measured by Li *et al.* [36] on EBIT with $n_e = 10^{10} \text{ cm}^{-3}$ and the energy of electron beam $E_e = 350 \text{ eV}$.

rate, the middle panel, Fig. 3(b), is the spectral intensity calculated by the CRM with the electron density $n_e = 10^{10} \text{ cm}^{-3}$ and the electron beam energy $E_e = 350 \text{ eV}$, and the bottom panel, Fig. 2(c), is the experimental spectra measured by Li *et al.* on the EBIT device with the electron density $n_e = 10^{10} \text{ cm}^{-3}$ and the energy of electron $E_e = 320$ and 310 eV [36]. Each individual transition was assumed to have the Gaussian profile with the FWHM 0.03 nm . The calculated spectrum of the W^{15+} ion is similar to the spectrum of the W^{14+} ion observed by Li *et al.* with EBIT [36]. To compare with the experimental spectra of Li *et al.* [36], the theoretical transition wavelengths are shifted to longer wavelengths by 0.20 nm . However, it should be verified by future experiments.

IV. CONCLUSION

In this paper, the $5p-5s$ transition spectra of $W \text{ XIV}-W \text{ XVI}$ ions have been calculated by the relativistic configuration in-

teraction method and collisional radiative model. The present theoretical results are in good agreement with the experimental results. The identification of the ionization degree from Li *et al.* seems lower by one than the present calculation and the observation of Kobayashi *et al.* The spectrum of $W \text{ XVI}$ has been calculated and compared with the results of Li *et al.* in the present work.

ACKNOWLEDGMENTS

This work was supported by the National Key Research and Development Program of China (Grant No. 2017YFA0402300), National Natural Science Foundation of China (Grants No. U1832126, No. 11874051, and No. 11775269), and Users with Excellence Program of Hefei Science Center CAS (Grant No. 2019HSC-UE014). X.B.D. would like to thank Dr. W. X. Li of Malmo University for providing their experimental data.

- [1] R. Neu, R. Dux, A. Kallenbach, T. Pütterich, M. Balden, J. C. Fuchs, A. Herrmann, C. F. Maggi, M. O'Mullane, R. Pugno, I. Radivojevic, V. Rohde, A. Sips, W. Suttrup, A. Whiteford, and the ASDEX Upgrade team, *Nucl. Fusion* **45**, 209 (2005).
- [2] G. F. Matthews, P. Coad, H. Greuner, M. Hill, T. Hirai, J. Likonen, H. Maier, M. Mayer, R. Neu, V. Philipps, R. Pitts, V. Riccardo, and JET-EFDA Contributors, *J. Nucl. Mater.* **390-391**, 934 (2009).
- [3] J. Roth, E. Tsitrone, T. Loarer, V. Philipps, S. Brezinsek, A. Loarte, G. F. Counsell, R. P. Doerner, K. Schmid, O. V. Ogorodnikova, and R. A. Causey, *Plasma Phys. Controlled Fusion* **50**, 103001 (2008).
- [4] Y. Ralchenko, J. Reader, J. M. Pomeroy, J. N. Tan, and J. D. Gillaspay, *J. Phys. B: At., Mol. Opt. Phys.* **40**, 3861 (2007).
- [5] G. Singh and N. K. Puri, *J. Phys. B: At., Mol. Opt. Phys.* **49**, 205002 (2016).
- [6] P. Quinet, *J. Phys. B: At., Mol. Opt. Phys.* **44**, 195007 (2011).
- [7] C. Fischer, G. Gaigalas, and P. Jönsson, *Atoms* **5**, 7 (2017).
- [8] M. S. Safronova, U. I. Safronova, S. G. Porsev, M. G. Kozlov, and Y. Ralchenko, *Phys. Rev. A* **97**, 012502 (2018).
- [9] U. I. Safronova and A. S. Safronova, *J. Phys. B: At., Mol. Opt. Phys.* **43**, 074026 (2010).
- [10] Y. Ralchenko, I. N. Draganic, J. N. Tan, J. D. Gillaspay, J. M. Pomeroy, J. Reader, U. Feldman, and G. E.

- Holland, *J. Phys. B: At., Mol. Opt. Phys.* **41**, 021003 (2008).
- [11] K. M. Aggarwal and F. P. Keenan, *At. Data Nucl. Data Tables* **111–112**, 187 (2016).
- [12] K. B. Fournier, *At. Data Nucl. Data Tables* **68**, 1 (1998).
- [13] Y. Podpaly, J. Clementson, P. Beiersdorfer, J. Williamson, G. V. Brown, and M. F. Gu, *Phys. Rev. A* **80**, 052504 (2009).
- [14] J. Sugar and V. Kaufman, *Phys. Rev. A* **12**, 994 (1975).
- [15] G. Veres, J. S. Bakos, and B. Kardon, *J. Quant. Spectrosc. Radiat. Transfer* **56**, 295 (1996).
- [16] J. Clementson, P. Beiersdorfer, E. W. Magee, H. S. McLean, and R. D. Wood, *J. Phys. B: At., Mol. Opt. Phys.* **43**, 144009 (2010).
- [17] F. G. Meijer, *Physica* **73**, 415 (1974).
- [18] A. N. Ryabtsev, E. Y. Kononov, R. R. Kildiyarova, W. L. Tchang-Brillet, and J. F. Wyart, *Phys. Scr.* **87**, 045303 (2013).
- [19] J. Clementson, T. Lennartsson, and P. Beiersdorfer, *Atoms* **3**, 407 (2015).
- [20] L. Iglesias, V. Kaufman, O. Garcia-Riquelme, and F. R. Rico, *Phys. Scr.* **31**, 173 (1985).
- [21] A. N. Ryabtsev, E. Y. Kononov, R. R. Kildiyarova, W. L. Tchang-Brillet, and J. F. Wyart, *Opt. Spectrosc.* **113**, 109 (2012).
- [22] A. Ryabtsev, E. Kononov, R. Kildiyarova, W. Tchang-Brillet, J. F. Wyart, N. Champion, and C. Blaess, *Atoms* **3**, 273 (2015).
- [23] M. Mita, H. Sakaue, D. Kato, I. Murakami, and N. Nakamura, *Atoms* **5**, 13 (2017).
- [24] J. O. Ekberg, R. Kling, and W. Mende, *Phys. Scr.* **61**, 146 (2000).
- [25] A. E. Kramida and T. Shirai, *At. Data Nucl. Data Tables* **95**, 305 (2009).
- [26] A. Kramida, *Can. J. Phys.* **89**, 551 (2011).
- [27] L. J. Curtis and D. G. Ellis, *Phys. Rev. Lett.* **45**, 2099 (1980).
- [28] C. E. Theodosiou and V. Raftopoulos, *Phys. Rev. A* **28**, 1186 (1983).
- [29] M. J. Vilkas, Y. Ishikawa, and E. Träbert, *Phys. Rev. A* **77**, 042510 (2008).
- [30] M. L. Qiu, R. F. Zhao, X. L. Guo, Z. Z. Zhao, W. X. Li, S. Y. Du, J. Xiao, K. Yao, C. Y. Chen, R. Hutton, and Y. Zou, *J. Phys. B: At., Mol. Opt. Phys.* **47**, 175002 (2014).
- [31] M. L. Qiu, W. X. Li, Z. Z. Zhao, Y. Yang, J. Xiao, T. Brage, R. Hutton, and Y. Zou, *J. Phys. B: At., Mol. Opt. Phys.* **48**, 144029 (2015).
- [32] H. A. Sakaue, D. Kato, N. Yamamoto, N. Nakamura, and I. Murakami, *Phys. Rev. A* **92**, 012504 (2015).
- [33] N. Nakamura, H. Kikuchi, H. A. Sakaue, and T. Watanabe, *Rev. Sci. Instrum.* **79**, 063104 (2008).
- [34] J. D. Silver, A. J. Varney, H. S. Margolis, P. E. G. Baird, I. P. Grant, P. D. Groves, W. A. Hallett, A. T. Handford, P. J. Hirst, A. R. Holmes, D. J. H. Howie, R. A. Hunt, K. A. Nobbs, M. Roberts, W. Studholme, J. S. Wark, M. T. Williams, M. A. Levine, D. D. Dietrich, W. G. Graham, I. D. Williams, R. O’Neil, and S. J. Rose, *Rev. Sci. Instrum.* **65**, 1072 (1994).
- [35] Y. Ralchenko, I. N. Draganić, D. Osin, J. D. Gillaspay, and J. Reader, *Phys. Rev. A* **83**, 032517 (2011).
- [36] W. Li, Z. Shi, Y. Yang, J. Xiao, T. Brage, R. Hutton, and Y. Zou, *Phys. Rev. A* **91**, 062501 (2015).
- [37] Y. Kobayashi, K. Kubota, K. Omote, A. Komatsu, J. Sakoda, M. Minoshima, D. Kato, J. Li, H. A. Sakaue, I. Murakami, and N. Nakamura, *Phys. Rev. A* **92**, 022510 (2015).
- [38] X. Ding, J. Yang, F. Koike, I. Murakami, D. Kato, H. A. Sakaue, N. Nakamura, and C. Dong, *J. Quant. Spectrosc. Radiat. Transfer* **204**, 7 (2018).
- [39] Z. Z. Zhao, M. L. Qiu, R. F. Zhao, W. X. Li, X. L. Guo, J. Xiao, C. Y. Chen, Y. Zou, and R. Hutton, *J. Phys. B: At., Mol. Opt. Phys.* **48**, 115004 (2015).
- [40] X. Ding, I. Murakami, D. Kato, A. H. Sakaue, F. Koike, and C. Dong, *Plasma Fusion Res.* **7**, 2403128 (2012).
- [41] X. Ding, J. Liu, F. Koike, I. Murakami, D. Kato, H. A. Sakaue, N. Nakamura, and C. Dong, *Phys. Lett. A* **380**, 874 (2016).
- [42] X. Ding, J. Yang, L. Zhu, F. Koike, I. Murakami, D. Kato, H. A. Sakaue, N. Nakamura, and C. Dong, *Phys. Lett. A* **382**, 2321 (2018).
- [43] Y. Ralchenko, *Plasma Fusion Res.* **8**, 2503024 (2013).
- [44] B. D. Van Sijde, J. J. A. M. Van der Mullen, and D. C. Schram, *Beitr. Plasmaphys.* **24**, 447 (1984).
- [45] K. B. Chai and D. H. Kwon, *J. Quant. Spectrosc. Radiat. Transfer* **227**, 136 (2019).
- [46] V. Jonauskas, Š. Masys, A. Kynienė, and G. Gaigalas, *J. Quant. Spectrosc. Radiat. Transfer* **127**, 64 (2013).
- [47] M. F. Gu, *Can. J. Phys.* **86**, 675 (2008).
- [48] X. Ding, F. Koike, I. Murakami, D. Kato, H. A. Sakaue, C. Dong, and N. Nakamura, *J. Phys. B: At., Mol. Opt. Phys.* **45**, 035003 (2012).
- [49] U. I. Safronova, A. S. Safronova, and P. Beiersdorfer, *Phys. Rev. A* **88**, 032512 (2013).